Biomaterials Science

PAPER

View Article Online
View Journal | View Issue

Cite this: *Biomater. Sci.*, 2016, **4**, 863

Regulation of breast cancer cell behaviours by the physical microenvironment constructed *via* projection microstereolithography†

Wenguang Yang,[a,b] Haibo Yu,*[a] Gongxin Li,[a,b] Bo Wang,[a,b] Yuechao Wang[a] and Lianqing Liu*[a]

Received 11th February 2016,
Accepted 22nd March 2016

DOI: 10.1039/c6bm00103c

www.rsc.org/biomaterialsscience

A considerable number of studies have examined how intrinsic factors regulate breast cancer cell behaviours; however, physical microenvironmental cues may also modulate cellular morphology, proliferation, and migration and mechanical properties. In the present study, the surrounding microenvironment of breast cancer cells was constructed using projection microstereolithography, enabling the investigation of the external environment's effects on breast cancer cell behaviours. A poly(ethylene) glycol diacrylate (PEGDA) solution was polymerized by programmable ultraviolet exposure to create arbitrary shapes with high biocompatibility, efficiency, flexibility and repeatability, and the resistance to cell attachment enabled the PEGDA coated film to hinder cell adhesion, allowing cells to grow in specific patterns. Furthermore, breast cancer cell morphology and mechanical properties were modified by altering the microenvironment. Proliferation was higher in breast cancer as compared to normal cells, consistent with the primary characteristic of malignant tumors. Moreover, breast cancer cells migrated more rapidly when grown in a narrow channel as compared to a wider channel. These findings enhance our understanding of the role of the microenvironment in breast cancer cell behaviours and can provide a basis for developing effective anticancer therapies.

Introduction

Breast cancer is among the most common types of cancer affecting about 12% of women worldwide.[1] As in other cancers, breast cancer develops as a result of interactions between environmental factors and susceptible cells. Recently, considerable attention has been paid to the regulation of breast cancer cell behaviours by intrinsic factors such as genetic and molecular scale functions.[2–6] In contrast, changes in the physical environment of tumours, while it is increasingly recognized that the microenvironment plays a key role in controlling cell fate by regulating cell behaviours,[7] are lacking effective research. Constructing an extracellular environment in which specific variables can be manipulated can provide insight into the mechanisms underlying interactions between breast cancer cells and their physical microenvironment.

Recently, the role of the physical microenvironment in influencing tumour cell behaviours including adhesion, morphology, differentiation, proliferation, migration and drug resistance has garnered increasing attention.[8–14] Gaining a greater understanding of extracellular microenvironmental cues, which physically modulate cancer initiation and progression, will contribute to our general understanding of breast cancer cells and help us to develop approaches for effective anticancer strategies.[15] To this end, engineered extracellular matrix (ECM) surfaces have proven useful in the investigation of interactions between tumour cells and their microenvironment.[16–18] Therefore, it is of great importance to construct a physical microenvironment wherein the behaviour of tumour cells can be regulated. The recent development of microfabrication techniques involving micro-post arrays,[19] micro-contact printing (μCP)[20–22] and fabrication of soft biocompatible substrates[22] and micro-fluidic channels[23,24] have enabled the construction of controllable physical microenvironments that can be altered to evaluate the contribution of external factors to tumour cell proliferation, migration and metastasis. Additionally, numerous studies on the engineering of specialty materials and systems have been conducted to examine the interactions between cancer cells and the microenvironment. Fibronectin contains short peptide sequences, such as arginine-glycine-aspartate (RGD), and is an ECM protein that binds other proteins and interacts with cells, to aid in cell adhesion, migration, and signaling.[25] A similar

[a]*State Key Laboratory of Robotics, Shenyang Institute of Automation, Chinese Academy of Sciences, Shenyang, 110016, P. R. China. E-mail: yangwenguang@sia.cn*
[b]*University of Chinese Academy of Sciences, Beijing 100049, P. R. China. E-mail: yuhaibo@sia.cn, lqliu@sia.cn*

†Electronic supplementary information (ESI) available. See DOI: 10.1039/c6bm00103c

method showed that ECM can guide the orientation of cell division.[26] Polydimethylsiloxane (PDMS)-based μCP was used to pattern ECM proteins onto nonadhesive substrates in order to study the role of cell–cell interactions in cell behaviours. This approach indicated that cell–cell contact can stimulate proliferation, which is consistent with many physiological processes.[18] However, the drying step in μCP may compromise the bioactivity of proteins and potential associated contamination may occur during the transfer of PDMS to the substrate.[27] Furthermore, these techniques involve the adsorption of specific proteins or the use of photolithography and soft lithography to guarantee cell adhesion and to set up the microenvironment; these are time-consuming and multistep processes that require specialized instrumentation, which therefore limits their wide application. To overcome these challenges, we developed a rapid, automated technique for creating a specific type of microenvironment for breast cancer cells. Polymerization of a poly(ethylene) glycol diacrylate (PEGDA) solution was induced by programmable ultraviolet (UV) exposure to create arbitrary patterns on glass surfaces. Bio-inert PEGDA surfaces resist protein adsorption and are considered unsuitable for cell adherence, while PEGDA uncovered glass allows cells to adhere and grow.

In this study, we focused on investigating the effects of physical extracellular microenvironmental cues on breast cancer cell progression using modified two-dimensional (2D) surfaces. We assessed breast cancer cell morphology, proliferation, mechanical properties and migration, without altering the physical and biochemical properties of the substrate. Our results suggest that breast cancer cells have a higher proliferation rate than normal cells and faster migration speed when growing in a narrow channel as opposed to a wider channel. Furthermore, we found that cell morphology and mechanical properties could be easily controlled by changing the microenvironment.

Results and discussion

Breast cancer cell morphology

By changing input image sequences, different virtual masks generated by a digital micromirror device (DMD) were utilized to fabricate configurable hydrogel microstructure patterns that are unsuitable for cell adherence. Mask projection stereolithography has been well developed for fabricating PEG-hydrogel microstructures. Liu *et al.* have fabricated hydrogel-based microvalves using masking techniques.[28] Lee *et al.* photopatterned PEG hydrogel microstructures modified with collagen to pattern cells.[29] Although the physical mask in most masking techniques used has been fabricated commercially, the time and cost of its fabrication process represent the main obstacles to rapid and inexpensive hydrogel microfabrication. Besides, it is not convenient to change masks during fabrication. To overcome these problems, Chen *et al.*[30] and we[31] have reported a projection printing system using digital micromirror devices instead of physical photomasks. Prior to printing, bitmap image sequences completely managed by a computer were input into the DMD. Being modulated using a DMD as a digital dynamic mask, polymerization of the pre-polymer solution can be induced to create arbitrary microstructures within several seconds (<5 s) in a single exposure. Thus, our method of fabricating PEG materials using the DMD is highly efficient, flexible and reproducible.

Fig. 1 shows the letters ("SIA") constructed by MCF-7 (breast cancer cells) in different fonts using a fabrication system known as "bio-writing". The letters were computer-generated and input into the DMD (Fig. 1c and f). Then, the corresponding pattern was projected onto the glass to generate hydrogel patterns. The MCF-7 cells adhered to hollow areas of the pattern (Fig. 1b and e) and fluorescence visualization was achieved by staining with calcein-AM (Fig. 1a and d). Moreover, cells that grew into the letter "I" showed a distinct morphology —that is, a higher length–width ratio as compared to those in other letters (Fig. 1d and e).

As shown in Fig. 1, the patterned PEGDA restricted the area in which the cells grew, and the shapes formed in the PEGDA hollow area can influence the cell morphology. This effect was shown to be closely related to the hollow shape of PEGDA structures. Consequently, we patterned a circular hollow PEGDA shape on common glass (Fig. 2a), and after a 2 day culture, the MCF-7 cell morphology was observed by fluorescence microscopy. In contrast to the well-spread cells grown on the common glass surface (Fig. 2d), cells cultured on the hollow PEGDA pattern formed an approximate circle (Fig. 2b and c).

In the common area, cells exhibited a well-spread morphology while those in the restricted area needed to adapt their shapes in order to survive. The deformed cells grew in restricted areas, indicating that the tumour cells were viable and strongly self-adaptive to the environment. However, cell morphology, which provides insight into the cytoskeletal status, is regulated by cellular protrusions.[32] And guiding of cytoskeletal alignments is often modulated by μCP. This technique is widely used to regulate cell morphology by the design features on the stamp, and to control the cell growth

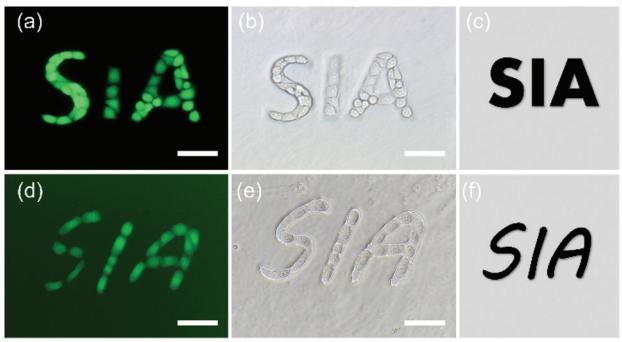

Fig. 1 Bio-writing using a DMD-based fabricating system. (a) and (d) Fluorescence images of cells stained with calcein-AM. (b) and (e) Corresponding optical light microscopy images. (c) and (f) The letters "SIA" have been input into the DMD in two different designed fonts. Scale bars are 100 μm.

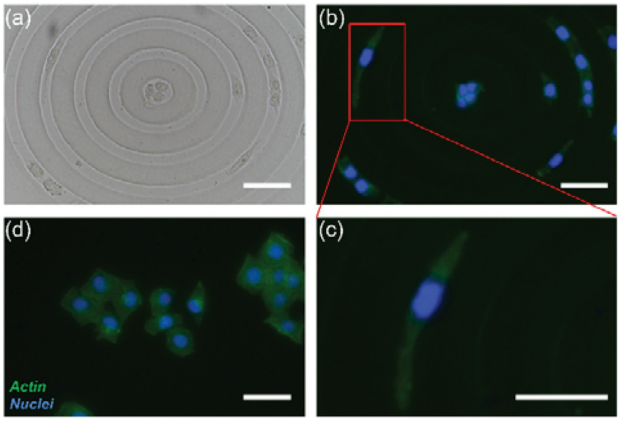

Fig. 2 Morphology of cells grown on a hollow circular PEGDA pattern. (a) Bright field image of cells growing in hollow areas of the PEGDA shape. (b) Corresponding fluorescence image, in which actin was stained in green, while the nuclei were stained in blue. (c) Cells cultured on the hollow PEGDA pattern formed an approximate circle. (d) Fluorescence images of cells grown on common glass. Scale bars are 30 μm.

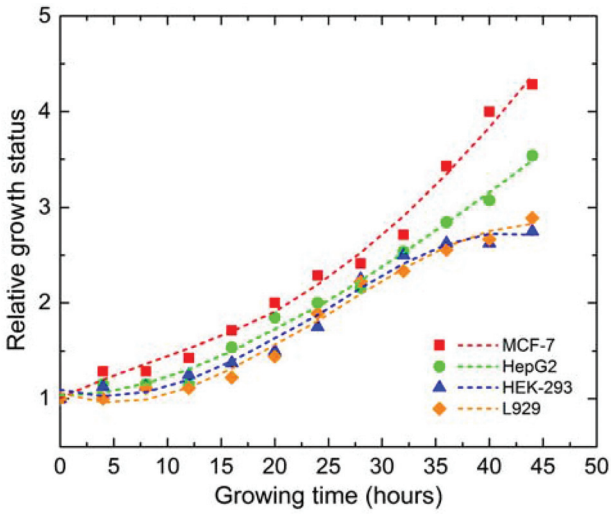

Fig. 3 Relative growth status of different cell types. Cancer cells (MCF-7 and HepG2) show a higher rate of proliferation than normal cells (HEK-293 and L929).

position.[33] However, as mentioned above, μCP is a complex and time-consuming experimental process relative to our simple and intuitive method. Furthermore, our method is straightforward and efficient for studying interactions between neighbouring cells, given their crucial role in determining the cell fate and function by forming cell chains.

Cell proliferation

To obtain detailed information on breast cancer cell growth properties on the patterned PEGDA shapes, in addition to MCF-7, three more types of cells (cancer cells control group: HepG2; non-cancerous cells control group: L929, HEK-293) cultured on glass were recorded in real time using optical microscopy. The growth behaviours of cells cultured for 40 h on glass modified with a hollow triangle-shaped PEGDA hydrogel were observed (ESI Fig. S1†). The confined hollow growth area allowed convenient observation of cell growth and proliferation. The growth process was divided into two phases: (1) cells selected the area to which they adhered and spread in the first 4 h; (2) cells began to proliferate until they covered the area that was not coated with the PEGDA hydrogel (ESI Movie S1†). During the first phase, after cells deposited onto the PEGDA-covered area, they migrated to the uncovered area and began to grow. The relative growth status (r) was estimated as follows:

$$r = \frac{\text{current cell number}}{\text{original cell number}} \quad (1)$$

The calculated values for relative growth status of different cells as shown in Fig. 3 indicated that the rate of proliferation was higher for the cancer cells than for normal cells, especially at later growth stages. Furthermore, after 12 h, the growth rate of all cell types increased, possibly due to cell–cell contact positively regulating proliferation and clusters of cells exhibiting enhanced proliferative activity.[18] At earlier stages of cell growth, cells were scattered in the restricted area without contacting other cells. However, over time, cells migrated and came into contact with other cells, which likely accelerated proliferation. Moreover, after 30 h, the proliferation rate of cancer cells including MCF-7 was higher than that of normal cells. Therefore, our experimental results demonstrated that the level of proliferative activity was higher in cancerous cells, which is consistent with invasion being a primary characteristic of malignant tumours. In contrast to traditional methods of observing the proliferation of cancer cells cultured in Petri dishes, our method restricted cell growth to specific areas, which enabled subsequent proliferation to be more accurately recorded.

Mechanical properties of patterned MCF-7 cells

In the cell proliferation experiment, we observed that MCF-7 cells were able to grow on the PEGDA surface when PEGDA-uncoated areas were filled and there was no remaining space for growth (ESI Fig. S2†). To investigate how the mechanical properties of MCF-7 cells were influenced by growth patterns, we used atomic force microscopy (AFM) to measure the Young's modulus of cells growing in different areas. As shown in Fig. 4a, MCF-7 cells were divided into three types: (1) cells that grew on common glass without restricted areas; (2) those that grew on the confined triangle pattern area; and (3) those that grew on the PEGDA surface. The results shown in Fig. 4b indicated that the average Young's modulus of freely growing cells was 3.3 ± 0.8 kPa, while cells growing in the restricted area had a higher value of 4.2 ± 1.1 kPa. In contrast, cells growing on the PEGDA surface were softer (ESI Fig. S3†). The mean value of Young's modulus of cells in different areas shows that the Young's modulus of most cells growing in the restricted area became larger than cells growing freely. As mentioned above, cells that grew in defined patterns modified their shapes to adapt to the restrictions imposed by their

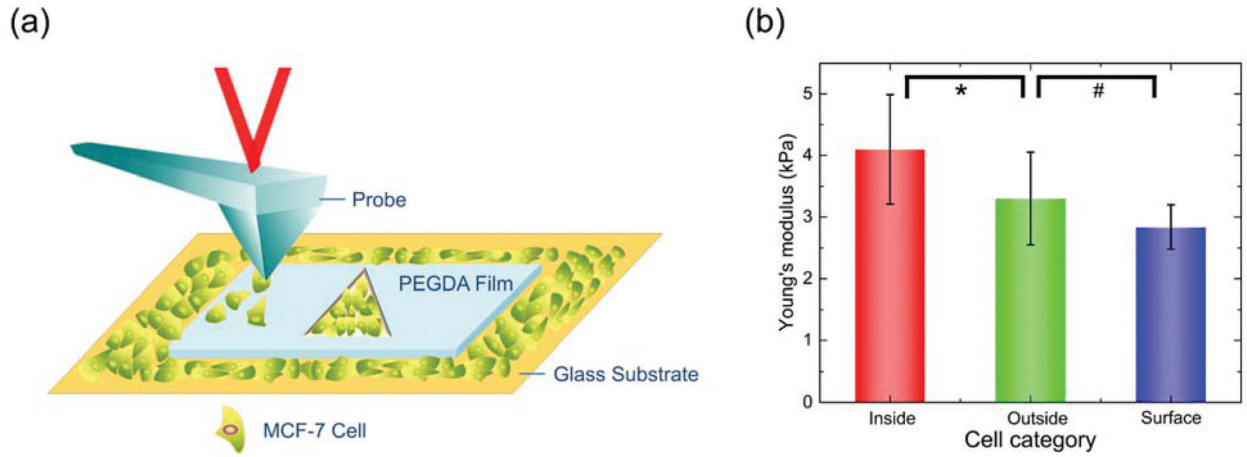

Fig. 4 Measured elastic modulus values for MCF-7 cells growing in different areas. (a) MCF-7 cells are able to grow on the PEGDA surface when cells filled the PEGDA-uncovered area. (b) Different Young's moduli for cells growing in different areas. Statistically different pairs ($p < 0.05$) are indicated by horizontal lines and either # or *.

environment. These processes were regulated by cytoskeletal deformation, and cells actively responded to the experimental conditions by changing their mechanical properties. This result suggested that patterned PEGDA limited the cell growth space and that restricted cells were required to change their cytoskeleton in order to adapt to the new circumstances. Moreover, cross-linked PEGDA was softer than the glass substrate, causing cells growing on the PEGDA surface to become less stiff than normal cells. Furthermore, these results suggest that MCF-7 cell morphology and mechanical properties can be easily regulated by the controlled physical microenvironment constructed by our method.

MCF-7 cell migration with tunable confinement

Cancer cells are able to travel through the walls of nearby blood vessels and migrate to other parts of the body including the lungs, liver, bones or brain through the vascular network. In order to investigate how the channel width affects cell migration, we fabricated honeycomb PEG channels which include three different widths: 10 μm, 20 μm and 30 μm. These PEG channels have the same height: ~30 μm (ESI Fig. S4†). The PEG film can hinder cell adhesion and cells were obliged to grow in the uncovered area (hollow area). And cell migration through different channel widths was continuously monitored by time-lapse microscopy to record cell motility. And the morphology of cells growing in different channels was obtained by scanning electron microscopy (SEM). MCF-7 cells grown in 30 μm channels exhibited a more widely spread structure as observed by SEM imaging; however, cells altered their morphologies to become elongated in order to adapt to the microenvironment of the 10 μm channel (Fig. 5).

The relationship between channel width and cell morphology was examined by staining the F-actin cytoskeleton of MCF-7 cells (Fig. 6). The aspect ratio of cells in the narrow channel became larger than that observed for cells growing in the wider channel as shown in Fig. 7c. Except for those in

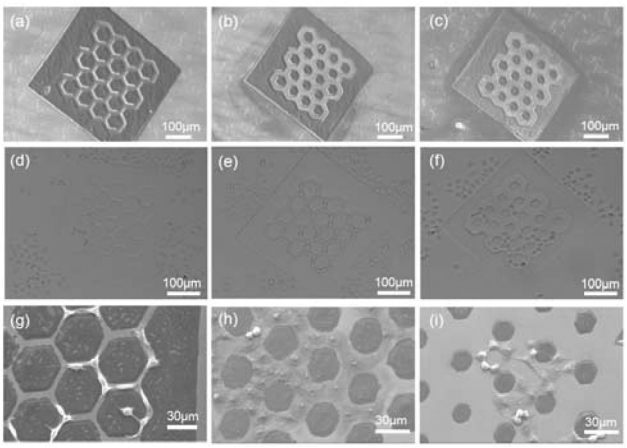

Fig. 5 SEM images of the fabricated PEGDA honeycomb microstructures with channels of different widths. (a)–(c) Fabricated channels with different widths: 10 μm, 20 μm, and 30 μm. (d)–(f) Optical light micrographs of MCF-7 cells growing in different channels. (g) and (h) SEM images of MCF-7 cells growing in different channels.

accord with our SEM results, fluorescence microscopy images revealed that the nuclei of cells in the narrow channel were deformed (Fig. 6a–c). To investigate the migration speeds of different cells in different channels, MCF-7 cells and other cells including cancer and normal cells were observed. As shown in Fig. 7a, the mean migration speeds of both MCF-7 and HeLa cells increased dramatically with decreasing channel width, which appears to be a linear relationship between the migration speeds in each of the channels. The maximum migration speed observed for MCF-7 cells was 17.6 ± 2.3 μm h^{-1}, corresponding to the 10 μm channel (ESI Movie S2†). In contrast, compared with cancer cells, the migration speed of normal cells was not related to channel width (Fig. 7b). In particular, HEK-293 cells migrated at a speed of 18.6 μm h^{-1} when growing in the widest channel (ESI Movies

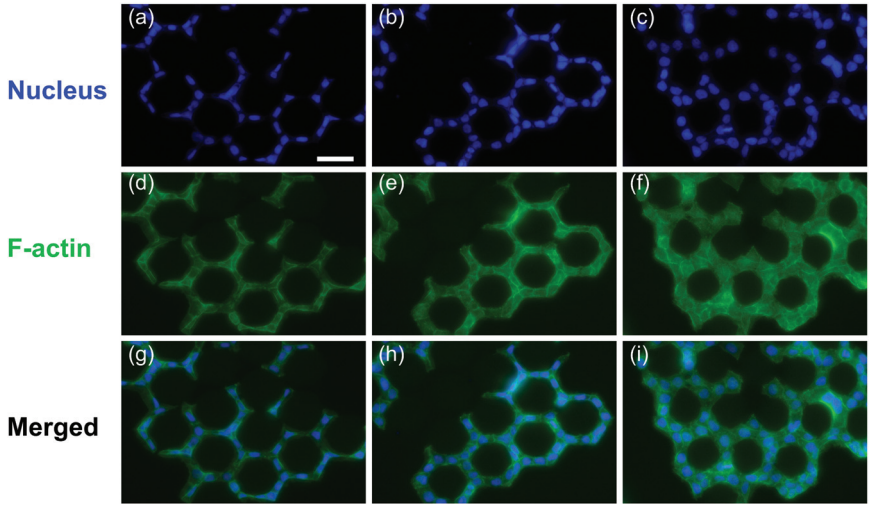

Fig. 6 Morphology of MCF-7 cells is controlled by different channels. Fluorescent microscopy images: (a)–(c) Nuclei were stained by DAPI. (d)–(f) F-actin was stained with CytoPainter Phalloidin-iFluor 488 Reagent. (g)–(i) Merged image, showing F-actin in green and nucleus in blue. Scale bar: 50 μm.

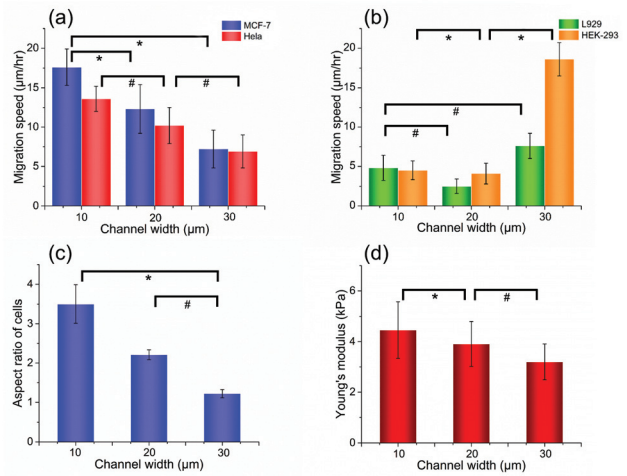

Fig. 7 Cell behaviours under tunable confinement. (a) Cancer cell migration speed *versus* different channel widths. (b) Normal cell migration speed in different channels. (c) Aspect ratio of MCF-7 cells which grew in different channels. (d) Mechanical properties of MCF-7 cells growing in different channels. Statistically different pairs ($p < 0.05$) are indicated by horizontal lines and either # or *.

S3 and S4†). In addition, the mechanical properties of MCF-7 cells growing in the narrow channel are stiffer than those of cells growing in the wider channel (Fig. 7d). During migration, a cell body must modify its shape and stiffness to interact with the surrounding tissue structure in order to migrate. The different migration speeds observed here may be explained by the effect of channel width on cytoskeletal architecture and the polarization of the traction force;[34,35] that is, the narrow channels are capable of regulating the traction force along the direction of the channel, thereby enhancing the migration speed.

Mesenchymal migration and amoeboid migration were proposed as the mechanisms for individual cells to study migration.[36] However, cancer cells exhibit both mesenchymal and amoeboid modes of migration; the mesenchymal-amoeboid transition (MAT) was used to explain cancer cell migration.[36–38] In the light of recent studies, two main factors driving the transition were identified: cell-intrinsic factors and extrinsic factors such as cell confinement and adhesion.[39] Considering that amoeboid migration mostly depends on cell body deformability, we constructed a tunable migrating channel to investigate the influence of physical confinement on the cell migration. It can be observed that cancer cells tended to deform their bodies to migrate in the narrow channel. As reported, non-cancer cells can first undergo mesenchymal migration, but they could eventually display amoeboid migration influenced by confinement.[38,40] Meanwhile, our results showed that normal cells (HEK-293) could migrate at a higher speed even faster than cancer cells, suggesting that they underwent the amoeboid migration facing specific confinement.

To confirm that cell migration required competent actin polymerization, we treated cells with cytochalasin B, which disrupts F-actin and inhibits new polymerization and then observed the cell migration speed. MCF-7 and HeLa cells were cultured in a 20 μm wide channel with different concentrations of cytochalasin B, and the migration speed of each cell was recorded. As shown in Fig. 8, cytochalasin B inhibited migration in a concentration-dependent manner up to 100 μg mL^{-1}, at which point cell migration was completely blocked. This indicated that actin played an important role in regulating cell migration.

Furthermore, an understanding of cell migration will be important in providing a biological framework for understanding cancer cell characteristics. Processes associated with cell migration including protrusion, adhesion and retraction are controlled by interactions that occur within the actin cytoskeletal structure. The cell membrane is coupled to a contrac-

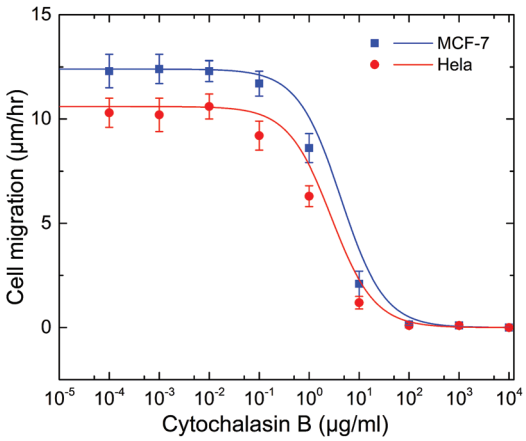

Fig. 8 Assessment of cytochalasin B impact on cancer cell migration.

tile cytoskeleton to generate hydrostatic pressure, which is enhanced by actin polymerization. Moreover, the flexibility and adaptability of the actin cytoskeleton interact with its surrounding environment through cell adhesion molecules. This activity regulates cell shape and enables force transmission to be the key driver of cell motility.[41] When exposed to different physical environments, migrating cells alter their cytoskeleton in response to changing physical environments, enabling them to adapt their shape as well as migration speed and direction. Furthermore, physical confinement induces F-actin remodeling[42,43] which alters the mechanical properties of cells, including the transfer of the actin monomer to the leading and trailing edges of cells as they migrate through narrow channels, which increases the speed of migration.

Tumour cell migration has been analysed using various experimental approaches, including micropipette,[44] micro-patterning,[45] wound healing,[46] microfluidics[47] and 3D ECM.[48] Compared with these techniques, our method using PEGDA solution polymerization can be used to create arbitrarily shaped microstructures with high efficiency, flexibility and repeatability, making it a more advantageous form of fabrication. We recognise that the two-dimensional (2D) substrates used in this study cannot fully mimic the complexity of the *in vivo* extracellular environment. However, 2D substrates have been widely used to investigate the mechanism of cell migration.[49] Migrating tumour cells may encounter 2D surfaces. In the bone metastasis, the surface of the trabecular bone may exhibit 2D conformations resulting in similar cellular interactions with the blood vessel wall.[50] Ongoing studies will involve construction of 3D hydrogel scaffolds in order to examine migratory trends in 3D matrices.

Conclusions

In this study, PEGDA patterns were fabricated using a DMD-based system, and their effects on breast cancer cell behaviours were examined. Compared to the existing methods, our technique is flexible, effective, and reproducible. Importantly, it offers the possibility of manipulating the substrate topography and thus the microenvironment of cancer cells, enabling the study of various cell behaviours. We found that cell migration through narrow fabricated channels was regulated by traction forces along the direction of the channel, which enhanced the migration speed. Cancer cells can alter their morphology and mechanical properties to adapt and survive; our method provides a tool to study breast cancer cell patterning and cell–cell interactions *in vitro*. Furthermore, given that targeting the tumour microenvironment is a feasible approach to cancer treatment, application of our method can contribute to a greater understanding of the behaviour of breast cancer cells and provide new insights into cancer progression as well as a basis for treatment strategies.

Experimental section

Projection microstereolithography system

ESI Fig. S5† shows an illustration of the experimental system for the assembly of the digitally light-addressable modification of the PEGDA hydrogel pattern. As shown, the digital mirror device (DMD)-based modulating projection printing system we developed consists of five parts: a UV laser (wavelength 375 nm, intensity range 0–50 mW), DMD, projection optics, computer controlled stages, and a charge-coupled device camera. The DMD, which is the key component of the system, serves as the dynamic mask and dynamically generates configurable images by digitally processing the projection light. To fabricate the PEGDA patterns, a series of programmable light patterns created by computer software were input into the DMD and then the corresponding images were projected onto the glass substrate through the projection optics. The detailed operating principle of the fabricating system and fabricating hydrogel microstructures has been described in our previous work.[31,51]

Materials

PEGDA (M_n = 700) and diphenyl(2,4,6-trimethylbenzoyl)-phosphine oxide (TPO) (both from Sigma-Aldrich, St Louis, MO, USA) were combined as a prepolymer solution as follows: pure PEGDA was mixed with ethyl alcohol in a ratio of 1 : 4 (v/v) and magnetically stirred for 30 min until the PEGDA was fully dissolved. The photoinitiator TPO was then added to the PEGDA/ethyl alcohol solution to obtain a concentration of 0.5% (w/v), with stirring for 30 min in the dark to ensure complete dissolution of the TPO.

The prepolymer solution was placed on the surface of the glass and cured by exposure to UV light. Upon absorption of the energy from UV radiation, free radicals were generated that broke the carbon–carbon bonds of the PEGDA chains, resulting in the conversion of the solution into a solid film.

Cell culture

MCF-7 breast cancer cells, HeLa human cervical cancer cells, and HepG2 hepatocellular carcinoma cells were cultured in Roswell Park Memorial Institute 1640 culture medium

(Hyclone, Logan, UT, USA) with 10% fetal bovine serum (FBS) and 1% penicillin/streptomycin in a 60 mm Petri dish at 37 °C and 5% CO_2. HEK-293 human embryonic kidney cells and L929 mouse fibroblasts were cultured in Dulbecco's Modified Eagle's Medium with high glucose supplemented with 10% FBS and 1% penicillin/streptomycin. Before culturing with hydrogel microstructures, cells were detached from the Petri dish by treatment with 0.25% trypsin/EDTA, followed by centrifugation for 3 min at 1000 rpm. The supernatant was removed and 1 ml of fresh culture medium was added to obtain a cell suspension. A 60 mm Petri dish was filled with 6 ml culture medium into which the glass substrate with the patterned PEGDA was submerged. A 200 μl volume of the cell suspension was added to the Petri dish, followed by incubation at 37 °C and 5% CO_2.

Microscopy, fluorescence staining and morphometric analysis

All live-cell and fluorescence imaging analyses were carried out using an Eclipse Ti microscope (Nikon, Tokyo, Japan) equipped with an incubator chamber that maintained a constant temperature, humidity, and CO_2 level.

For fluorescence staining, cells were washed twice with phosphate-buffered saline (PBS), and then fixed with 4% paraformaldehyde in PBS for 15–20 min. Fixed cells were rinsed two or three times in PBS with 0.1% Triton X-100 for 10 min at room temperature to increase permeability. To label F-actin, 100 μl of CytoPainter Phalloidin-iFluor 488 Reagent (Abcam, Cambridge, UK) was added to the cells at room temperature for 20–90 min. After removing excess phalloidin conjugate, nuclei were stained by adding 0.5 μg ml^{-1} 4′,6-diamino-2-phenylindole (DAPI; Sigma-Aldrich) for 10 min.

For cell pattern visualization, cells were treated with calcein-AM (Sigma-Aldrich, St Louis, MO, USA) as follows. The glass with patterned cells was washed with PBS, followed by addition of calcein-AM to the PBS solution at a final concentration of 2 μmol l^{-1} and incubation for 15 min in the CO_2 incubator. Cells were visualized using an epifluorescence microscope. Cell spreading measurements and image analysis were carried out using ImageJ software (National Institutes of Health, Bethesda, MD, USA). Cell elongation was described by the aspect ratio, which was defined as the major axis divided by the minor axis of elliptical cells.

Measurement of mechanical properties

AFM was used to determine the mechanical properties of cells (Bioscope Catalyst; Bruker, Camarillio, CA, USA). In order to mimic the pH and ionic conditions of cultured cells, force mapping was carried out in PBS (pH 7.4). Measurements were made in fluidic contact mode, and all force curves of each cell were determined at different positions, with 20 force curves obtained at the same loading rate. The elastic modulus of the cell was calculated using the Hertz model.[52]

Measurement of the migration speed of cells

Cells measurements were obtained during the moving phase. As evidenced in the video recordings (ESI Fig. S6 and Movies S2–S4†), cells assumed a round shape when movement ceased; this enabled us to determine the cell status (migrating or proliferating). We selected the center of the cell (black symbol) as the measuring point. Although cells showed different degrees of spreading, the distance moved was independent of cell size. We did not take into account the effects of cell size on the measurements (ESI Fig. S7†).

Statistical analysis

All data are reported as the mean ± standard error of the mean. Sample means were compared using analyses performed by ANOVA, followed by Tukey's *post hoc* test. $P < 0.05$ was considered to be statistically significant.

Acknowledgements

This research work was partially supported by the National Natural Science Foundation of China (project no. 61302003, 61475183 and 61503258), and the CAS FEA International Partnership Program for Creative Research Teams.

Notes and references

1 A. McGuire, J. Brown, C. Malone, R. McLaughlin and M. Kerin, *Cancers*, 2015, **7**, 908–929.
2 G. L. Semenza, *Biochim. Biophys. Acta, Mol. Cell Res.*, 2015, **3**, 382–391.
3 M. E. Barnard, C. E. Boeke and R. M. Tamimi, *Biochim. Biophys. Acta, Rev. Cancer*, 2015, **1856**, 73–85.
4 A. Rizwan, M. Cheng, Z. M. Bhujwalla, B. Krishnamachary, L. Jiang and K. Glunde, *Breast Cancer*, 2015, 1.
5 J. G. Jackson, X. H. Zhang, T. Yoneda and D. Yee, *Oncogene*, 2001, **20**, 7318–7325.
6 S. Paruthiyil, H. Parmar, V. Kerekatte, G. R. Cunha, G. L. Firestone and D. C. Leitman, *Cancer Res.*, 2004, **64**, 423–428.
7 W. F. Liu and C. S. Chen, *Mater. Today*, 2005, **8**, 28–35.
8 B. G. Chung and J. Choo, *Electrophoresis*, 2010, **31**, 3014–3027.
9 S. Wang, H. Wang, J. Jiao, K. J. Chen, G. E. Owens, K. Kamei, J. Sun, D. J. Sherman, C. P. Behrenbruch, H. Wu and H. R. Tseng, *Angew. Chem.*, 2009, **48**, 8970–8973.
10 N. Iida, A. Dzutsev, C. A. Stewart, L. Smith, N. Bouladoux, R. A. Weingarten, D. A. Molina, R. Salcedo, T. Back, S. Cramer, R. M. Dai, H. Kiu, M. Cardone, S. Naik, A. K. Patri, E. Wang, F. M. Marincola, K. M. Frank, Y. Belkaid, G. Trinchieri and R. S. Goldszmid, *Science*, 2013, **342**, 967–970.
11 H. Jeon, S. Koo, W. M. Reese, P. Loskill, C. P. Grigoropoulos and K. E. Healy, *Nat. Mater.*, 2015, **14**, 918–923.
12 T. F. Gajewski, H. Schreiber and Y. X. Fu, *Nat. Immunol.*, 2013, **14**, 1014–1022.
13 S. P. Carey, C. M. Kraning-Rush, R. M. Williams and C. A. Reinhart-King, *Biomaterials*, 2012, **33**, 4157–4165.

14 T. Q. Huang, X. Qu, J. Liu and S. Chen, *Biomed. Microdevices*, 2014, **16**, 127–132.
15 D. E. Ingber, *Semin. Cancer Biol.*, 2008, **18**, 356–364.
16 S. P. Palecek, J. C. Loftus, M. H. Ginsberg, D. A. Lauffenburger and A. F. Horwitz, *Nature*, 1997, **385**, 537–540.
17 F. Re, A. Zanetti, M. Sironi, N. Polentarutti, L. Lanfrancone, E. Dejana and F. Colotta, *J. Cell Biol.*, 1994, **127**, 537–546.
18 C. M. Nelson and C. S. Chen, *FEBS Lett.*, 2002, **514**, 238–242.
19 S. Y. Tee, J. P. Fu, C. S. Chen and P. A. Janmey, *Biophys. J.*, 2011, **100**, L25–L27.
20 S. J. Han, K. S. Bielawski, L. H. Ting, M. L. Rodriguez and N. J. Sniadecki, *Biophys. J.*, 2012, **103**, 640–648.
21 R. S. Kane, S. Takayama, E. Ostuni, D. E. Ingber and G. M. Whitesides, *Biomaterials*, 1999, **20**, 2363–2376.
22 D. E. Discher, P. Janmey and Y. L. Wang, *Science*, 2005, **310**, 1139–1143.
23 Y. K. Cheung, E. U. Azeloglu, D. A. Shiovitz, K. D. Costa, D. Seliktar and S. K. Sia, *Angew. Chem., Int. Ed.*, 2009, **48**, 7188–7192.
24 A. Pathak and S. Kumar, *Proc. Natl. Acad. Sci. U. S. A.*, 2012, **109**, 10334–10339.
25 E. Ruoslahti and B. Obrink, *Exp. Cell Res.*, 1996, **227**, 1–11.
26 M. Thery, V. Racine, A. Pepin, M. Piel, Y. Chen, J. B. Sibarita and M. Bornens, *Nat. Cell Biol.*, 2005, **7**, 947–953.
27 K. Glasmastar, J. Gold, A. S. Andersson, D. S. Sutherland and B. Kasemo, *Langmuir*, 2003, **19**, 5475–5483.
28 R. H. Liu, Q. Yu and D. J. Beebe, *J. Microelectromech. Syst.*, 2002, **11**, 45–53.
29 J. Y. Lee, S. S. Shah, J. Yan, M. C. Howland, A. N. Parikh, T. Pan and A. Revzin, *Langmuir*, 2009, **25**, 3880–3886.
30 C. Cha, P. Soman, W. Zhu, M. Nikkhah, G. Camci-Unal, S. Chen and A. Khademhosseini, *Biomater. Sci.*, 2014, **2**, 703–709.
31 W. Yang, H. Yu, W. Liang, Y. Wang and L. Liu, *Micromachines*, 2015, **6**, 1903–1913.
32 H. Y. Yu, K. P. Lim, S. J. Xiong, L. P. Tan and W. Shim, *Adv. Healthcare Mater.*, 2013, **2**, 1188–1197.
33 D. E. Ingber, *Polym. Surf. Interfaces*, 1997, 413–424.
34 D. Yamazaki, S. Kurisu and T. Takenawa, *Cancer Sci.*, 2005, **96**, 379–386.
35 T. F. Gajewski, H. Schreiber and Y.-X. Fu, *Nat. Immunol.*, 2013, **14**, 1014–1022.
36 Y.-J. Liu, M. Le Berre, F. Lautenschlaeger, P. Maiuri, A. Callan-Jones, M. Heuzé, T. Takaki, R. Voituriez and M. Piel, *Cell*, 2015, **160**, 659–672.
37 K. Wolf, I. Mazo, H. Leung, K. Engelke, U. H. Von Andrian, E. I. Deryugina, A. Y. Strongin, E.-B. Bröcker and P. Friedl, *J. Cell Biol.*, 2003, **160**, 267–277.
38 J. Guck, F. Lautenschläger, S. Paschke and M. Beil, *Integr. Biol.*, 2010, **2**, 575–583.
39 T. Lämmermann and M. Sixt, *Curr. Opin. Cell Biol.*, 2009, **21**, 636–644.
40 P. Friedl, *Curr. Opin. Cell Biol.*, 2004, **16**, 14–23.
41 C. D. Madsen, S. Hooper, M. Tozluoglu, A. Bruckbauer, G. Fletcher, J. T. Erler, P. A. Bates, B. Thompson and E. Sahai, *Nat. Cell Biol.*, 2015, **17**, 68–80.
42 E. M. Balzer, Z. Q. Tong, C. D. Paul, W. C. Hung, K. M. Stroka, A. E. Boggs, S. S. Martin and K. Konstantopoulos, *FASEB J.*, 2012, **26**, 4045–4056.
43 K. M. Stroka, Z. Z. Gu, S. X. Sun and K. Konstantopoulos, *Curr. Opin. Cell Biol.*, 2014, **30**, 41–50.
44 L. Soon, G. Mouneimne, J. Segall, J. Wyckoff and J. Condeelis, *Cell. Motil. Cytoskeleton*, 2005, **62**, 27–34.
45 A. C. von Philipsborn, S. Lang, J. Loeschinger, A. Bernard, C. David, D. Lehnert, F. Bonhoeffer and M. Bastmeyer, *Development*, 2006, **133**, 2487–2495.
46 K. J. Simpson, L. M. Selfors, J. Bui, A. Reynolds, D. Leake, A. Khvorova and J. S. Brugge, *Nat. Cell Biol.*, 2008, **10**, 1027–1038.
47 W. J. Polacheck, J. L. Charest and R. D. Kamm, *Proc. Natl. Acad. Sci. U. S. A.*, 2011, **108**, 11115–11120.
48 F. Sabeh, R. Shimizu-Hirota and S. J. Weiss, *J. Cell Biol.*, 2009, **185**, 11–19.
49 A. J. Ridley, M. A. Schwartz, K. Burridge, R. A. Firtel, M. H. Ginsberg, G. Borisy, J. T. Parsons and A. R. Horwitz, *Science*, 2003, **302**, 1704–1709.
50 K. Anselme, A. Ponche and M. Bigerelle, *Proc. Inst. Mech. Eng., Part H*, 2010, **224**, 1487–1507.
51 W. Yang, H. Yu, F. Wei, G. Li, Y. Wang and L. Liu, *Biomed. Microdevices*, 2015, **17**, 1–8.
52 A. Touhami, B. Nysten and Y. F. Dufrene, *Langmuir*, 2003, **19**, 4539–4543.

